A Marie-Curie-ITN
within H2020

Proceedings of the International Symposium on
Thermal Effects in Gas flows In Microscale
October 24-25, 2019 – Ettlingen, Germany

ISTEGIM2019: 283836

COUPLED THERMAL TRANSPORT AND MASS DIFFUSION DURING VAPOR ABSORPTION INTO SESSILE LIQUID DESICCANT DROPLETS

Zhenying Wang[1,2], Daniel Orejon[1,3], Khellil Sefiane[1,3], Yasuyuki Takata*[1,2]
[1]International Institute for Carbon-Neutral Energy Research (WPI-I[2]CNER), Kyushu University, Japan
[2]Department of Mechanical Engineering, Thermofluid Physics Laboratory, Kyushu University, Japan
z.wang@heat.mech.kyushu-u.ac.jp, takata@mech.kyushu-u.ac.jp
[3]Institute for Multiscale Thermofluids, School of Engineering, University of Edinburgh, UK
d.orejon@ed.ac.uk, K.Sefiane@ed.ac.uk

KEY WORDS

heat and mass transfer, IR thermography, absorptive heating, evaporative cooling, vapor pressure difference

ABSTRACT

Introduction

Liquid desiccant is a type of aqueous salt solution [1] characterized by its hygroscopic properties widely applied in dehumidification and absorption systems. By taking advantage of the vapor absorption capability of liquid desiccants, further optimization of indoor environment control, energy conservation and emission reduction, has been pursued. In the abovementioned practical systems, the heat and mass transfer between liquid desiccant and humid air (or water vapor) is paramount. This has gained increasing attention from researchers in the field of energy system design and optimization. Nevertheless, despite the numerous existing studies on dehumidification devices mainly at the macroscale, the behavior of single liquid desiccant droplets in contact with humid air has been scarcely reported. In this study, we investigate the heat and mass transport coupling mechanisms [2] during vapor absorption into lithium bromide desiccant (LiBr-H_2O) droplets for controlled environmental conditions. The evolution of droplet profile and the temperature distribution at the droplet surface are investigated using optical imaging and infrared (IR) thermography. The physical process that ensues along with vapor absorption are compared to that of water droplet evaporation.

Experimental Setup

Experiments are conducted within an environmental chamber with accurately controlled conditions (800L, -20 ~ 100 °C, 20 ~ 98% *RH*, PR-3KT from ESPEC Corp.). Fig. 1 shows the experimental setup for this study. During experiments, the evolution of droplet profile is recorded with a high-definition CCD camera (Sentech STC-MC152USB with a RICOH lens and 25-mm spacing ring) at 4.8 fps, and an LED backlight is applied to enhance the image contrast. An IR camera, FLIR SC-4000 with a spectral range between 3.0 and 5.0 μm and a resolution of 18 mK, is setup vertically looking at the substrate from the top. Thermal evolution at the droplet liquid-gas interface is recorded at 2 fps. 54 wt.% LiBr-H_2O solution from Sigma-Aldrich is used as the testing fluid for vapor absorption experiments. Contrast experiments of droplet evaporation are conducted using distilled water (Sigma-Aldrich). Smooth polytetrafluoroethylene (PTFE) (S_q = 0.357μm), a commonly used

* Corresponding author

material in dehumidification systems, is applied as the testing substrate, and the volume of the droplet is controlled as 3.2 ± 0.3 μL with diameters of 2.07~2.2 mm.

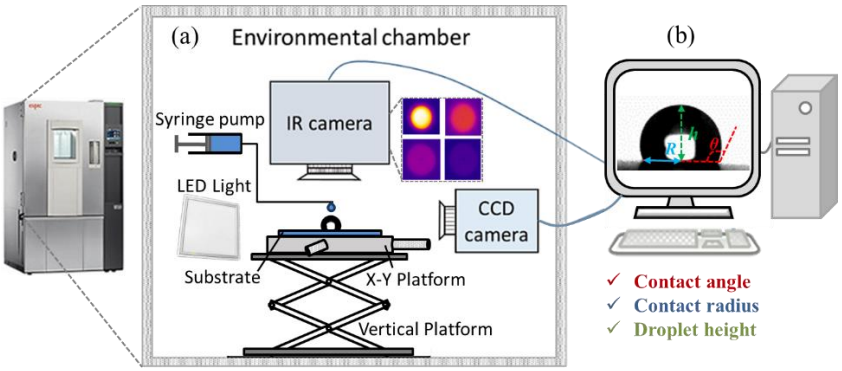

Figure 1: Overview of the experimental setup. (a) Experimental setup: environmental chamber, CCD camera, IR camera, back light, stainless steel vertical platform, droplet dosing system; (b) Data acquisition system with ImageJ® and Matlab®.

Results and Discussion

Shown in Fig. 2, the volume of LiBr-H_2O droplets increases following a saturation trend as vapor absorption goes on, while the volume of pure water droplets decreases due to water evaporation, and the decreasing trend is close to linear. Moreover, the rates of vapor absorption and evaporation depend greatly on the experimental air condition.

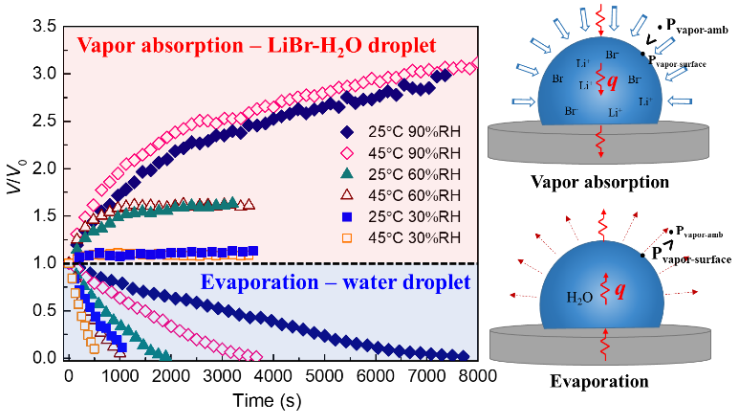

Figure 2: Evolution of non-dimensional droplet volume with respect to the original volume, V/V_0, along with time, t (s), during vapor absorption and evaporation for the six environmental conditions.

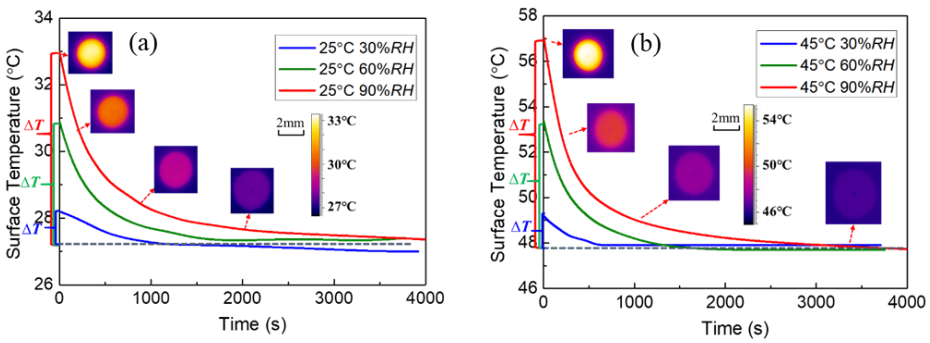

Figure 3: Evolution of average temperature at the droplet surface and corresponding IR images during vapor absorption for ambient conditions of 30% *RH*, 60% *RH*, 90% *RH*, and (a) 25 °C, (b) 45 °C.

Fig. 3 indicates the distribution and evolution of droplet interfacial temperature along with time. The spatial temperature distribution across the LiBr-H_2O droplet is overall homogenous, while the average surface

temperature varies slowly along with time. The droplet surface experiences the highest temperature right after being deposited on the substrate. This indicates that vapor absorption starts as the droplet is generated from the needle and gets contact with humid air. The released heat due to vapor-to-water phase change causes the observed temperature increase when respect to ambient conditions. After being deposited on the substrate, the absorbed heat is dissipated both through heat conduction towards the substrate, and through convective heat transfer into the ambient air. As a combined result of heat dissipation and decreasing absorption rate, the droplet surface gradually cools down towards equilibrium with the ambient. In the case of pure water, droplets experience the lowest surface temperature right after being deposited due to evaporative cooling, then gradually warm up as they reach equilibrium with the substrate and the ambient.

By making use of Eq. (1), we calculated the absorptive/evaporative heat flux at the first instants right after droplet deposition.

$$\Phi_q = \frac{\dot{Q}}{S} = \frac{L_{vl}\rho\frac{dV}{dt}}{\pi\left(h^2+R^2\right)}, \tag{1}$$

where Φ_q represents the average heat flux across the droplet surface, kW/m^2, $\dot{Q}$ is the rate of heat flow, kW, S represents the area of droplet surface, m^2, and L_{vl} is the latent heat released during vapor-liquid phase change, kJ/kg. The calculation results are listed in Tab. 1. Results show that the heat flux induced by absorptive heating depends greatly on the ambient condition. For LiBr-H_2O droplets, the absorptive heat flux follows the order of $\Phi_{q,45°C90\%RH} > \Phi_{q,45°C60\%RH} > \Phi_{q,25°C90\%RH} > \Phi_{q,25°C60\%RH} > \Phi_{q,25°C30\%RH} \approx \Phi_{q,45°C30\%RH}$, which corresponds with the order of initial temperature rise for the six experimental conditions. Since vapor absorption is driven by the vapor pressure difference between the ambient and the droplet surface, at low relative humidity conditions, *i.e.*, small gradient of concentration, the vapor absorption rate is rather low, hence small absorptive heat flux is reported. For pure water droplets, the vapor pressure difference is small for high relative humidity conditions, resulting in the small evaporation rate and weak evaporative cooling effect in such cases.

Φ_q (kW/m^2)	25°C30%*RH*	25°C60%*RH*	25°C90%*RH*	45°C30%*RH*	45°C60%*RH*	45°C90%*RH*
LiBr-H_2O droplet	0.507	1.066	1.166	0.472	1.512	1.771
Pure water droplet	1.132	0.812	0.216	2.848	1.443	0.333

Table 1: Average heat flux, Φ_q (kW/m^2), at the interface of LiBr-H_2O droplets and pure water droplets induced by absorption heating and evaporation cooling, respectively.

The vapor pressure at the droplet interface, $P_{vapor,surface}$, can be further evaluated according to the fitting correlations derived by Patek and Klomfar (Eqs. (2) and (3)) [3].

$$P_{vapor,surface} = P_{sat}\left(\Theta\right), \tag{2}$$

where P_{sat} is the saturation vapor pressure of pure water at "shifted temperature", Θ, due to the presence of dissolved salts. Θ is function of the mole fraction, x_{mole}, and temperature, T, of LiBr-H_2O solution, and can be calculated as Eq. (3).

$$\Theta = T - \sum_{i=1}^{8} a_i \left(x_{mole}\right)^{m_i} \left|0.4 - x_{mole}\right|^{n_i} \left(\frac{T}{T_c}\right)^{t_i}, \tag{3}$$

where T_c is the critical temperature of pure water, 647.096 K, a = {-2.41303×10^2, 1.91750×10^7, -1.75521×10^8, 3.25432×10^7, 3.92571×10^2, -2.12626×10^3, 1.85127×10^8, 1.91216×10^3}, m = {3, 4, 4, 8, 1, 1, 4, 6}, n = {0, 5, 6, 3, 0, 2, 6, 0}, t = {0, 0, 0, 0, 1, 1, 1, 1}, and the mole fraction, x_{mole}, is calculated by Eq. (4).

$$x_{mole} = \frac{x/M_{\mathrm{LiBr}}}{x/M_{\mathrm{LiBr}} + (1-x)/M_{\mathrm{H_2O}}}, \tag{4}$$

where x is the mass fraction of LiBr solute in LiBr-H_2O solution, and M represents the molar mass. Since the initial concentration of the LiBr-H_2O solution is known, any increase in the droplet volume is due to water absorbed, from experimental observations of droplet profile evolution in time, the mass fraction of LiBr can be estimated.

Then, combining Eqs. (2)-(4), the vapor pressure difference can be calculated. Fig. 4(a) shows the evolution of vapor pressure difference between the droplet interface and ambient air during vapor absorption. From experimental observations of droplet profile, the vapor absorption rate is estimated in time, which is presented in Fig. 4(b). It shows that the vapor pressure differences and absorption rates are the largest right after droplet deposition. Moreover, the order of initial vapor pressure difference, $\Delta P|_{45°C90\%RH} > \Delta P|_{45°C60\%RH} > \Delta P|_{25°C90\%RH} > \Delta P|_{25°C60\%RH}$, corresponds with the order of initial vapor absorption rate for the four experimental conditions, $dV/dt|_{45°C90\%RH} > dV/dt|_{45°C60\%RH} > dV/dt|_{25°C90\%RH} > dV/dt|_{25°C60\%RH}$. As vapor absorption proceeds, the salt concentration within the droplet decreases, therefore the vapor pressure difference between the ambient and the droplet surface diminishes and so does the vapor absorption rate.

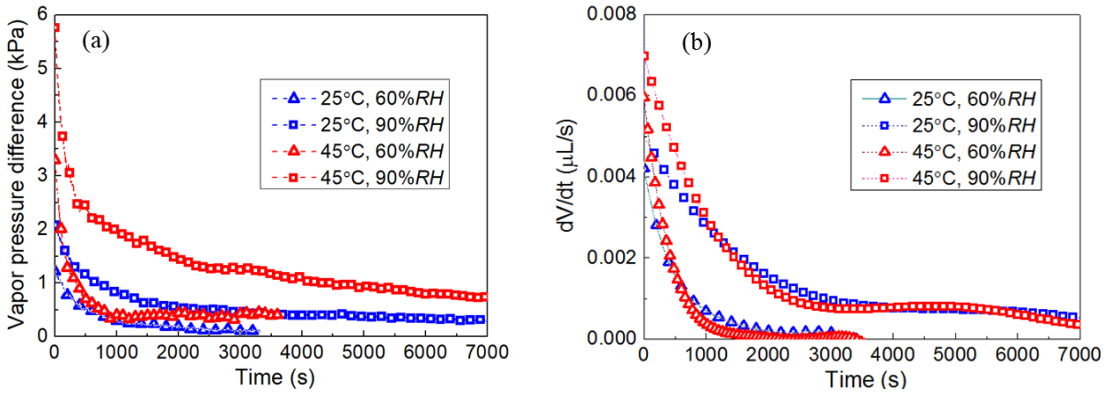

Figure 4: Evolution of (a) calculated vapor pressure difference, ΔP (kPa), between the droplet interface and ambient air, and (b) rate of droplet volume increase, dV/dt (μL/s) during vapor absorption on PTFE substrates.

Conclusion

The coupled heat and mass transfer process during vapor absorption into LiBr-H_2O droplet is experimentally investigated under controlled environmental conditions. Results show that the droplets experience the highest surface temperature right after being deposited on the substrate, and then gradually cool down as a combined result of the decreasing vapor absorption rate and the heat dissipation into the substrate and into the ambient. Moreover, the initial temperature rise at the droplet surface quantitatively agrees with the absorptive heat flux depending on the ambient conditions studied. Along with water uptake, the desiccant solution gets gradually diluted, and the vapor pressure difference between the ambient air and the droplet surface decreases along with time, which explains the saturation increasing trend of droplet volume along with time. Findings presented here provide a valuable extension to existing literature of phase change at the droplet scale, which contributes to a more complete understanding of the role of liquid desiccant droplets in dehumidification processes.

Acknowledgements

The authors gratefully acknowledge the supports received from the International Institute for Carbon-Neutral Energy Research (WPI-I^{2}CNER) and JSPS KAKENHI (Grant no. JP16K18029 and JP18K13703).

References and Citations

[1] Chua, K. J., Chou, S. K., & Yang, W. M. (2016). Liquid desiccant materials and dehumidifiers – A review. *Renewable & Sustainable Energy Reviews*, **56**,179-195.

[2] Wang, Z., Orejon, D., Sefiane, K., & Takata, Y. (2019). Coupled thermal transport and mass diffusion during vapor absorption into hygroscopic liquid desiccant droplets. *International Journal of Heat and Mass Transfer*, **134**, 1014-1023.

[3] Patek, J., & Klomfar, J. (2006). A computationally effective formulation of the thermodynamic properties of LiBr–H_2O solutions from 273 to 500 K over full composition range. *International Journal of Refrigeration*, **29.4**, 566-578.